Engineering Geology 361 (2026) 108504

Contents lists available at ScienceDirect

Engineering Geology

journal homepage: www.elsevier.com/locate/enggeo

Contribution of time-evolving landslide sources to the anomalous tsunami observed in the 2024 Noto earthquake☆

Ming-Jen Lo [a], Tso-Ren Wu [b,c,d,*], Kenji Satake [a,d,e]

[a] Department of Earth Sciences, National Central University, Taoyuan City, Taiwan
[b] Graduate Institute of Hydrological and Oceanic Sciences, National Central University, Taoyuan City, Taiwan
[c] Department of Civil Engineering, National Central University, No. 300, Jhongda Rd., Jhongli District, Taoyuan City 320317, Taiwan
[d] Earthquake-Disaster & Risk Evaluation and Management Center, E-DREaM, National Central University, No. 300, Jhongda Rd., Jhongli District, Taoyuan City 320317, Taiwan
[e] Earthquake Research Institute, The University of Tokyo, Tokyo, Japan

ARTICLE INFO

Keywords:
Submarine landslide
Bottom displacement rates
The 2024 Noto earthquake and tsunami

ABSTRACT

On January 1, 2024, a powerful earthquake (M 7.6) struck the Noto Peninsula, Japan, triggering a tsunami in the Sea of Japan. In Toyama Bay, the tsunami arrived earlier than expected. This study investigates the 2024 Noto tsunami event by separately modeling three potential tsunami generation mechanisms: vertical displacement from fault motion, horizontal displacement, and submarine landslides. To enhance the accuracy of submarine landslide-induced tsunami modeling, a computational fluid dynamics model, SPLASH3D, is utilized to simulate the landslide dynamics and determine its duration. Subsequently, a temporally variable seabed motion is used as the initial condition for a tsunami simulation code, COMCOT, to generate a dynamic tsunami source. The simulation results indicate that the sliding process has a significant influence on the observed tsunami in Toyama Bay, producing waveforms that better match observations than those derived from the equivalent instantaneous initial free surface displacement method. The combined simulation of dynamic submarine landslides, vertical displacements from fault motion, and horizontal displacements of the Noto Peninsula closely matches the observed data, enabling a detailed analysis of each source's contribution to the anomalous tsunami. Simulation results indicate that the submarine landslide was responsible for the early arrival of the tsunami. The contributions of the vertical fault displacement and submarine landslide each account for approximately 45 % of the maximum wave height, elucidating the unexpectedly high tsunami wave height. Therefore, the risks posed by landslide-generated tsunamis constitute a critical issue that must be addressed in tsunami early warning and coastal engineering risk assessment.

1. Introduction

At 16:10:22.5 (Japan Standard Time: UTC + 9) on January 1, 2024, a powerful earthquake with a magnitude of Mw 7.5 (or Japan Meteorological Agency magnitude Mj 7.6) struck the Noto Peninsula in Japan. The epicenter was located in Suzu City, Ishikawa Prefecture (coordinates: 37.495°N, 137.27°E), with a focal depth of 16 km (Japan Meteorological Agency [JMA], 2024). According to the JMA, seismic intensity 7 was recorded in Monzen Town, Wajima City, and Kano, Shika Town, Ishikawa Prefecture (seismic intensities in this paper are measured on the JMA scale). Several other locations on the Noto Peninsula experienced intensity 6-upper, and Intensity 6-lower was observed in a wider area, including Niigata Prefecture.

The Noto region has been experiencing a seismically active period since December 2020, characterized by what has been termed the "Noto Earthquake Swarm" (Fujii and Satake, 2024; JMA, 2024). Between the end of 2020 and the end of 2023, a total of 506 earthquakes with a maximum seismic intensity of 1 or greater were recorded in the region (JMA, 2024).

The powerful mainshock on January 1 also triggered a tsunami that affected the coastlines along the Sea of Japan. At 16:12, shortly after the event, the JMA issued a tsunami warning for the coastal regions of Niigata (inclusive of Jo-Chu-Kaetsu and Sado Island), Toyama, and both Noto and Kaga coasts of Ishikawa Prefecture. At the same time, tsunami

☆ This article is part of a Special issue entitled: 'Seismic & Secondary Hazards' published in Engineering Geology.

* Corresponding author at: Graduate Institute of Hydrological and Oceanic Sciences, National Central University, Taoyuan City, Taiwan.
E-mail address: tsoren@ncu.edu.tw (T.-R. Wu).

https://doi.org/10.1016/j.enggeo.2025.108504
Received 28 July 2025; Received in revised form 11 November 2025; Accepted 8 December 2025
Available online 11 December 2025

advisories were issued for the Sea of Japan coasts of southern Hokkaido, Aomori, Akita, Yamagata, Fukui, Kyoto, northern Hyogo, Tottori, Shimane (including Oki Islands), and Yamaguchi Prefectures. Additionally, tsunami forecasts (indicating slight sea level changes) were announced for the central and western Pacific coasts of Hokkaido, the northern Sea of Japan coast of Hokkaido, the coast along the Sea of Okhotsk, the Pacific coast of Aomori, Mutsu Bay, the Sea of Japan coasts of Fukuoka and Saga Prefectures, the western coast of Nagasaki, and the Iki and Tsushima Islands.

At 16:22, the tsunami warning for the Noto coast in Ishikawa Prefecture was upgraded to Major Tsunami Warning. Simultaneously, the tsunami advisories for Yamagata, Fukui, and northern Hyogo Prefectures were upgraded to tsunami warnings. Furthermore, the tsunami forecasts for the western Pacific coast and the northern coast of the Sea of Japan, including Hokkaido, the coasts of Fukuoka and Saga, and the Iki–Tsushima region, were elevated to tsunami advisories.

At 20:30, the Major Tsunami Warning for Noto was downgraded to a tsunami warning. By 01:15 on January 2, all tsunami warnings were downgraded to tsunami advisories. At 02:30, the tsunami advisories for the Sea of Japan coasts of Fukuoka and northern Saga were lifted and changed back to tsunami forecasts. At 07:30, tsunami advisories for the Sea of Japan coast of Yamaguchi and Oki Islands in Shimane were also lifted. Finally, by 10:00 a.m., all tsunami advisories were lifted and returned to forecast status (JMA, 2024).

The tide gauge data from the Japan Meteorological Agency show that a tsunami wave height of 80 cm was recorded in Kanazawa City, Ishikawa Prefecture. In comparison, Sakata City in Yamagata Prefecture observed a wave height of approximately 80 cm. At Wajima Port, Ishikawa Prefecture, a maximum wave height exceeding 120 cm was recorded at one point; however, subsequent assessments concluded that this data may have been affected by local ground uplift or instrumental malfunction and was thus deemed invalid (JMA, 2024).

The tide gauge station at Nagahashi in Suzu City ceased operation immediately after the earthquake. Aerial surveys conducted by the GSI revealed that ground uplift in the area caused the tide gauge to rise above the water surface, preventing it from recording accurate sea level data (JMA, 2024).

According to the field survey report by the JMA's Mobile Survey Team, estimated tsunami heights were reported for various locations near the affected coastal areas. The maximum runup height was recorded at Funami Park in Jōetsu City, Niigata Prefecture, at an elevation of 6.2 m above sea level (Heidarzadeh et al., 2024). The highest trace height was found on a building in Shiramura, Noto Town, Ishikawa Prefecture, at an elevation of 4.7 m above sea level. However, in Wajima Port and the Nagahashi area of Suzu City, where reliable observation data were lacking, no visible traces of tsunami inundation were identified (JMA, 2024). Similar field survey results were also reported by the Japan Society of Coastal Engineers (Yuhi et al., 2024).

Additionally, the Association of Japanese Geographers (2024), in collaboration with the GSI, analyzed aerial photographs to map the flooded areas. It was estimated that approximately 190 ha of land were inundated by the tsunami. Regarding the absence of inundation traces around Wajima Port and Nagahashi, researchers hypothesized that the phenomenon may be attributed to crustal uplift caused by the earthquake. The uplifted coastline may have acted as a natural seawall, reducing the impact of the tsunami on these areas (The Association of Japanese Geographers, 2024).

During this event, the tsunami behavior observed along the Toyama Bay coast exhibited anomalous characteristics. At Toyama Tide Station (located in Toyama City) and Fushiki Tide Station (located in Takaoka City, Fig. 1), approximately 80 km from the epicenter, tsunami arrival was initially expected around 10 min after the earthquake. However, Toyama station detected tsunami waves just 3 min after the mainshock, and Fushiki station did so only 2 min after (Fig. 2). This unexpectedly early arrival quickly drew attention from both the media and academic communities. It was widely recognized that, in addition to the tsunami

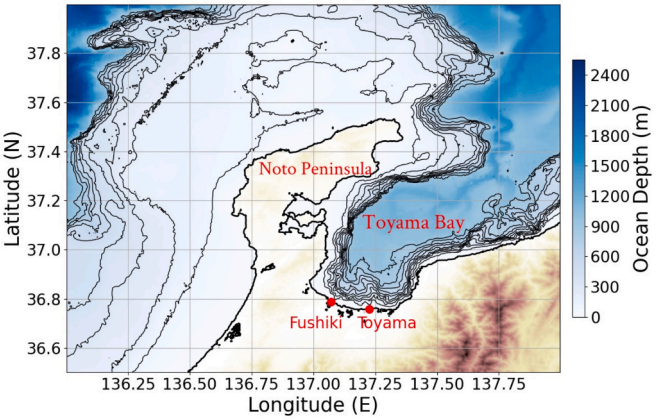

Fig. 1. The bathymetry map of Noto Peninsula, Toyama Bay and the locations of the Toyama and Fushiki tide gauge stations.

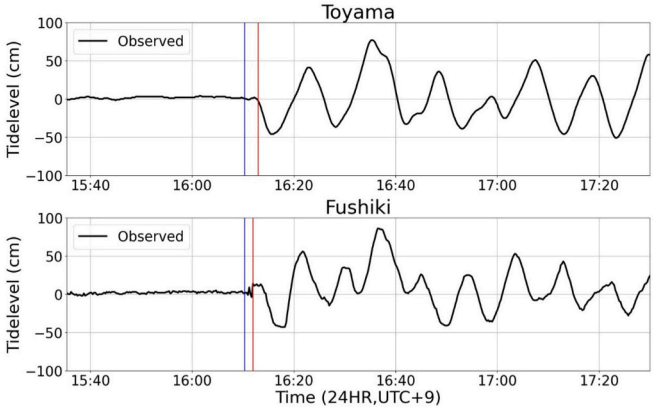

Fig. 2. Tsunami waveforms observed at the Toyama and Fushiki tide gauge stations. The blue vertical line indicates the earthquake origin time; the red vertical lines mark the tsunami arrival times at each station. (For interpretation of the references to colour in this figure legend, the reader is referred to the web version of this article.)

generated by seafloor displacement from fault motion, other tsunami sources may have contributed to the observed phenomenon (JMA, 2024; Mulia et al., 2024; Yanagisawa et al., 2024).

Within the Engineering Geology context, landslide-generated impulse waves and their coupling with ambient water have been increasingly examined using complementary modeling frameworks—from Tsunami Squares (TS) formulations that parameterize slide–water momentum exchange to high-fidelity Reynolds-Averaged Navier–Stokes (RANS)/Smoothed Particle Hydrodynamics (SPH) reconstructions of historical events (Franco et al., 2021; Liu et al., 2025; Wang et al., 2019, 2021). These studies show that push-ahead/drag-along interactions and entry kinematics can strongly amplify near-field wave heights and alter arrival times, with implications for hazard assessment in confined embayments and bays. While these papers treat subaerial landslide, this paper propose a new method for submarine landslide.

Recent studies by Mulia et al. (2024) and Yanagisawa et al. (2024) both suggest that submarine landslides contributed to the anomalous tsunami behavior observed in Toyama Bay. Their respective simulation results demonstrate that landslide-induced tsunamis can indeed lead to earlier wave arrival times. These findings suggest that submarine landslides played a critical role in the tsunami anomalies observed during the 2024 Noto earthquake.

It is noteworthy that during the 2007 Noto Peninsula earthquake (Mw 6.9), a tsunami was also observed to arrive earlier than expected in

Toyama Bay. (Abe et al., 2008) hypothesized that the presence of submarine landslides within Toyama Bay may explain this phenomenon, and that the earthquake possibly triggered such landslides.

2. Source of abnormal tsunamis observed in Toyama Bay

Current tsunami simulations generated by earthquakes typically account only for vertical seafloor displacements from the fault motion, which cause uplift of the free water surface. However, in addition to vertical displacements, horizontal displacements can also generate tsunamis, particularly in areas with steep submarine topography, as demonstrated by Tanioka and Satake (1996).

In the 2024 event, horizontal displacements of approximately 80 cm were observed near the Noto Peninsula side of Toyama Bay, while displacements of about 10 cm were recorded on the Toyama side of the bay (GSI, 2024). The seafloor in Toyama Bay is characterized by steep slopes, fulfilling the conditions proposed in the aforementioned study.

Another potential factor that could generate a tsunami in this event is submarine landslides. Toyama Bay, with its steep seafloor topography, is known to be prone to such submarine landslides. In earlier studies of anomalous tsunamis (Mulia et al., 2024; Yanagisawa et al., 2024), researchers often employed inverse modeling based on observed tsunami waveforms. By incorporating existing bathymetric data and known locations of submarine landslides, they estimated the likely sites of submarine landslides. Subsequent adjustments were made to the size and geometry of the landslide blocks in the simulation until the resulting tsunami waveforms closely matched those recorded by tide gauge stations. This approach was used to infer the most plausible locations and scales of the submarine landslides responsible for generating the tsunami.

Following the earthquake, the Japan Coast Guard [JCG] conducted a series of surveys in Toyama Bay (JCG, 2024a, 2024b). These included post-earthquake bathymetric surveys using seafloor sonar, which were compared with bathymetric data collected by the Hokuriku Regional Development Bureau in 2010. The results revealed several clear indications of submarine landslides:

(1) A survey published on January 24, 2024, identified a submarine landslide zone located approximately 4 km north of the Toyama tide gauge station. This feature was found at water depths ranging from 260 to 330 m and measured approximately 500 m in length, 80 m in width, and up to 40 m in thickness.
(2) A subsequent survey released on December 2, 2024, revealed multiple submarine landslide scars near the coast of Fushiki in Takaoka City (less than 3 km from shore), spanning water depths of approximately 15 to 350 m. The affected area stretched roughly 3 km in the north–south direction and 0.5 km east–west. The report highlighted two particularly prominent landslide sites within this zone. Both were of similar scale, with estimated dimensions of 200–250 m in length, 10–20 m in width, and 5–10 m in thickness.

Although the findings confirmed that submarine landslides occurred after 2010, a direct causal link to the 2024 Noto earthquake had not been firmly established. The relationship between the 2024 Noto earthquake and submarine landslides became clear with the release of a joint survey report on January 16, 2025, by the University of Toyama, Kyoto University, and Kanazawa University (University of Toyama, 2025). The investigation employed uncrewed underwater vehicles (UUVs) to conduct photographic surveys of the seafloor near the mouths of the Jinzu River (adjacent to the Toyama tide gauge station) and the Oyabe and Shō Rivers (near the Fushiki tide gauge station).

The results revealed that both submarine landslides were composed of semi-consolidated terrestrial sedimentary layers that had collapsed. The exposed fracture surfaces appeared fresh, with no signs of weathering or biological colonization. These observations strongly suggest that the landslides were recent events, most likely triggered by the 2024 Noto earthquake.

With sufficient data now available regarding submarine landslides, this study aims to conduct numerical tsunami simulations based on verified parameters. The simulations incorporate multiple tsunami sources, including vertical displacement due to fault motion, horizontal displacement, and submarine landslides. The resulting waveforms are then compared against tide gauge records to evaluate the contribution of each tsunami source and better understand the mechanisms behind the observed anomalies.

3. Simulation method

3.1. Shallow water equations in COMCOT

In this study, we employed the COMCOT (Cornell Multi-grid Coupled Tsunami Model) code to separately simulate tsunamis generated by vertical displacement, tsunamis induced by horizontal displacement, and tsunamis generated by landslides. The model is designed to simulate various mechanisms for generating tsunamis, including fault dislocation, submarine landslides, and other potential sources of tsunamis. COMCOT can solve both linear and nonlinear forms of the shallow water equations and has been successfully applied to the reconstruction and analysis of multiple historical tsunami events (Liu et al., 1995; Wang and Liu, 2005; Wu et al., 2008), making it suitable for this study.

COMCOT is based on the Shallow Water Equations (SWE), which govern the motion of long waves influenced by gravity, inertia, and seabed topography. For cases in which the water depth is significantly greater than the wave height, the model treats tsunamis as linear shallow water waves. However, in shallow coastal regions where wave amplitudes grow and nonlinear effects become significant, COMCOT can switch to the nonlinear form of the SWE to more accurately simulate wave propagation and transformation.

The linear SWE are as follows:

$$\frac{\partial \eta}{\partial t}+\frac{1}{R\cos\varphi}\left[\frac{\partial P}{\partial \psi}+\frac{\partial}{\partial \varphi}(\cos\varphi Q)\right]=0$$

$$\frac{\partial P}{\partial t}+\frac{gh}{R\cos\varphi}\frac{\partial \eta}{\partial \psi}-fQ=0 \tag{1}$$

$$\frac{\partial Q}{\partial t}+\frac{gh}{R}\frac{\partial \eta}{\partial \varphi}+fP=0$$

Where η is the free surface height, R is the radius of the Earth, φ is the latitude, ψ is the longitude, P is the zonal momentum flux, Q is the meridional momentum flux, h is the static water depth, g is the gravitational acceleration, and f is the Coriolis parameter.

For vertical displacement-generated tsunamis and tsunamis induced by horizontal displacement, we adopted the initial free surface displacement method. This approach is computationally efficient and requires fewer parameters. However, when applying the same method to simulate submarine landslide-induced tsunamis, we observed significant discrepancies between the simulated waveforms and tide gauge observations. This phenomenon is primarily because landslide-generated tsunami sources typically exhibit much shorter wavelengths and involve stronger vertical accelerations compared to tsunamis generated by vertical displacements. As a result, relying on the initial free surface displacement method, which neglects the dynamic nature of the source process, can lead to significant modeling inaccuracies. The omission of time-dependent bottom motion fails to capture the transient energy transfer from the landslide to the water column, thereby underestimating the wave amplitude and misrepresenting the overall wave field, particularly in the near field.

To address this issue, we incorporated a three-dimensional computational fluid dynamics (CFD) model, SPLASH3D, into our workflow. The 3D model provides a more comprehensive representation of

hydrodynamic mechanisms, enabling more accurate simulation of near-field flow fields. However, full-scale, high-resolution 3D simulations of landslide-generated tsunamis are computationally expensive and currently infeasible for large domains.

3.2. Incompressible Navier-Stokes equation in SPLASH3D

SPLASH3D is a three-dimensional multiphase fluid dynamics model developed based on the Truchas framework from the Los Alamos National Laboratory (LANL). It incorporates multiple advanced modules to simulate complex flow phenomena with high accuracy.

The model is based on the incompressible Navier–Stokes equations (Wu, 2004) as its core formulation. To track the free surface interface between fluids, SPLASH3D utilizes the Volume of Fluid (VOF) method while employing the Finite Volume Method (FVM) for spatial discretization. This combination enables precise simulation of a wide variety of complex flows, including ocean waves, river currents, moving solid boundaries, and non-Newtonian fluids. These advantages make it particularly well-suited for simulating the dynamics of submarine landslides in the context of this study.

The governing equations in SPLASH3D are:

(1) Mass Conservation Equation (Incompressibility Condition):

$$\vec{\nabla} \bullet \vec{u} = 0 \tag{2}$$

Here, $\vec{u} = \vec{u}(x, y, z, t)$ represents the velocity vector field.

(2) Momentum Conservation Equation (Navier–Stokes Equation):

$$\frac{\partial \vec{u}}{\partial t} + (\vec{u} \bullet \vec{\nabla})\vec{u} = -\frac{1}{\rho}\nabla p + \nu \nabla^2 \vec{u} + \vec{f} \tag{3}$$

Where ρ is the fluid density (assumed constant for incompressible flow), p is the pressure, ν is the kinematic viscosity ($\nu = \mu/\rho$, with μ being the dynamic viscosity), and $\vec{f}$ represents the body forces (such as gravity or other external forces).

3.3. Hybrid approach

We adopted a hybrid approach that combines the strengths of both 2D (COMCOT) and 3D (SPLASH3D) models. For the 2D modeling component, we implemented the sliding mass approach in COMCOT using the temporally variable seabed motion method, rather than the initial free surface displacement method. This technique is based on the formulation proposed by Watts et al. (2003), which can model the dynamic landslide-generated tsunami sources more accurately than using the initial free surface displacement method. In this framework, bottom displacement rates (dh/dt) are computed and introduced at each time step to represent the dynamic bottom motion induced by the landslide. Compared to the initial free surface displacement method, this method provides a more realistic representation of the energy release process associated with landslides, while preserving computational efficiency.

4. Tide gauge and bathymetric data

The tide gauge data used in this study were primarily obtained from the Japan Meteorological Agency (JMA, 2024).

For the seafloor topography, this study utilized the GEBCO, 2023 dataset provided by the General Bathymetric Chart of the Oceans (GEBCO). The dataset has a spatial resolution of 0.25 arc-minutes and was extracted for the domain spanning 35.0°N to 40.0°N and 134.0°E to 140.0°E (GEBCO, 2023). This domain encompasses the entirety of the Noto Peninsula and Toyama Bay—key areas affected by the 2024 event. The resolution of the GEBCO dataset is sufficient to support high-resolution tsunami simulations (0.5 arc-minutes) conducted with the COMCOT model.

5. Simulation parameters

5.1. Vertical fault displacement-generated tsunami parameters

For the vertical displacement-generated tsunami, the initial free surface deformation was constructed using Okada's formula (Okada, 1985).

The fault parameters used in this study are based on the fault model released by the GSI (GSI, 2024), which represents the latest available analysis as of that date. This report provides detailed horizontal and vertical surface displacement data that serve as the basis for fault inversion analysis, outlining three fault segments derived from the inversion results.

To simulate the vertical displacement-generated tsunami, we adopted the parameters from these three fault segments as specified in the GSI model.

GSI's fault model is derived from two main observational techniques for estimating crustal deformation:

(1) GNSS (Global Navigation Satellite System) measurements collected via Japan's electronic control points, which provide high-precision vertical and horizontal displacement data.
(2) SAR (Synthetic Aperture Radar) satellite imagery, used to supplement and integrate surface deformation information.

Table 1 shows the parameters of the three faults:

5.2. Horizontal displacement-generated tsunami parameters

For the tsunami generated by horizontal displacement, the initial free surface deformation was constructed based on the formulation proposed by Tanioka and Satake (1996).

Along the coastal area of the Noto Peninsula facing Toyama Bay, horizontal displacements of approximately 80–100 cm directed toward the west-northwest were observed. On the coast of Toyama Bay in Toyama Prefecture, the observed displacements were approximately 10 cm, primarily directed northwest (GSI, 2024).

Given the significant spatial variation in horizontal displacements around Toyama Bay, the horizontal displacement-generated tsunami simulation was divided into two sub-regions, each with distinct displacement characteristics:

(1) Noto Peninsula side of Toyama Bay: An initial free surface deformation was generated based on a horizontal displacement of 0.8 m directed at 290° (Fig. 3 left).
(2) Toyama Prefecture side of Toyama Bay: An initial free surface deformation was generated based on a horizontal displacement of 0.1 m directed at 315° (Fig. 3, right).

This partitioned approach allows a more accurate representation of spatially heterogeneous crustal movements and their contributions to tsunami generation in Toyama Bay.

5.3. Submarine landslide tsunami parameters

For submarine landslide-generated tsunami simulations, we used COMCOT's temporally variable seabed motion method to represent the landslide dynamics. This method is based on the formulation by Watts et al. (2003), which allows for the progressive release of landslide energy to be included at each time step.

To apply the temporally variable seabed motion method, additional landslide parameters are required, including the geometry of the slide body (length, width, and thickness), its initial and final positions, the slope gradient, and the duration of motion. All parameters except the

Table 1
Parameters of faults.

	Lon (°E)	Lat (°N)	Depth of top (km)	Length (km)	Width (km)	Strike (°)	Dip (°)	Slip (°)	Dislocation (m)	Magnitude (Mw)
Fault 1	136.680	37.246	0.1	22.0	12.2	22.7	40.6	84.4	6.79	7.09
Fault 2	136.876	37.414	0.0	16.2	20.4	78.3	54.9	140.2	2.83	6.90
Fault 3	137.037	37.445	0.1	66.8	11.5	53.3	49.7	114.6	4.42	7.27

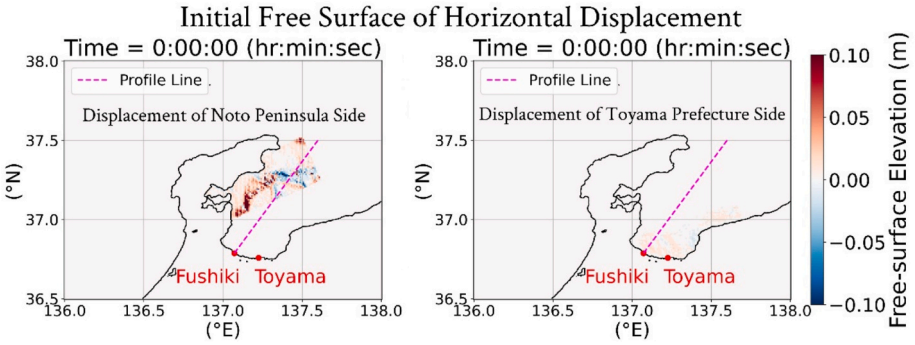

Fig. 3. Initial free surface generated by horizontal displacement of 0.8 m along the Noto Peninsula coastal side of Toyama Bay (left) and 0.1 m along the Toyama coastal side of Toyama Bay (right).

duration can be inferred from the Japan Coast Guard's post-earthquake bathymetric surveys. To estimate the landslide duration, we conducted dedicated 3D SPLASH3D simulations of the identified submarine landslide events. The output from these simulations was then used as a reference for assigning landslide duration in the COMCOT-based simulations.

5.3.1. Site and scale of submarine landslide

This study conducted numerical tsunami simulations for two submarine landslide zones that have been well-documented through detailed field investigations (Fig. 4):

(1) Near the mouth of the Jinzu River, located approximately 4 km from the Toyama tide gauge station.
(2) Near the mouths of the Oyabe and Shō Rivers, located within 3 km of the Fushiki tide gauge station.

The positions and dimensions of the landslide sources were configured based on the latest survey data. Each landslide source was individually simulated to evaluate its influence on the nearest tide gauge station.

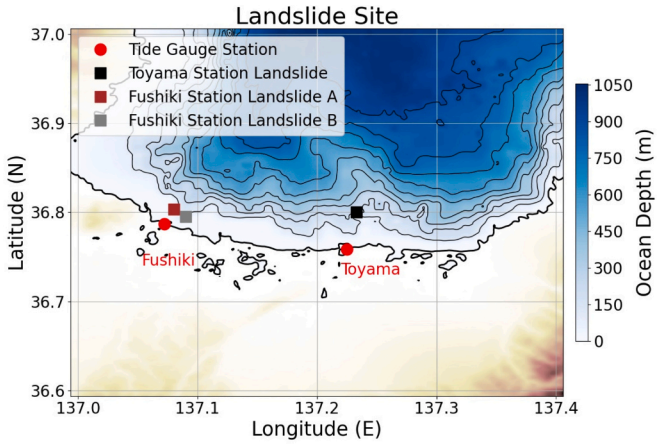

Fig. 4. Landslide sites and location of tide gauge stations.

5.3.2. Duration of submarine landslide

To estimate the duration of submarine landslides, which is typically not available in survey reports, we conducted high-resolution dynamic simulations using SPLASH3D. This CFD-based approach enables a detailed reconstruction of the time-dependent behavior of submarine landslides, particularly those resulting from the collapse of semi-consolidated sedimentary layers.

For this study, we focused on simulating landslide motion along the x–z plane (perpendicular to the axis of the submarine canyon) to analyze the horizontal and vertical dynamics of the landslide process. The computational domain was designed with a spatial resolution of 1 m × 100 m × 1 m in the x, y, and z directions, respectively, allowing for fine resolution in both the slope-normal and vertical dimensions.

The seafloor topography was constructed based on bathymetric profiles from post-earthquake surveys conducted by the Japan Coast Guard. The submarine canyon geometry was approximated by combining multiple solid rectangular blocks. The landslide body was modeled as a rectangular fluid block, measuring 50 m × 50 m in the x–z plane, with a density of 2 g/cm^3, representing the dislodged rock mass triggered by the earthquake.

SPLASH3D enables detailed tracking of the dynamic evolution and physical quantities associated with submarine landslides over time. Fig. 5 presents a simulated scenario in which earthquake-induced sediment failure triggers a submarine landslide. By evaluating the total kinetic energy throughout the simulation, the duration of the energy-releasing phase of the landslide can be estimated.

Simulation results showed that the landslide block reached its maximum kinetic energy around 10 s after initiation, driven by gravitational acceleration. Between 20 and 30 s, the block maintained relatively strong kinetic activity, although a gradual decrease in energy was observed. After 30 s, deposition began, and the kinetic energy declined rapidly until the landslide came to a complete stop.

Based on these results, we set the landslide duration for subsequent tsunami modeling to be within the range of 20 to 30 s. This range was further adjusted to more accurately reflect local seafloor slope angles, thereby improving the accuracy of landslide tsunami simulations.

Table 2 shows the parameters of submarine landslide for the temporally variable seabed motion method in COMCOT:

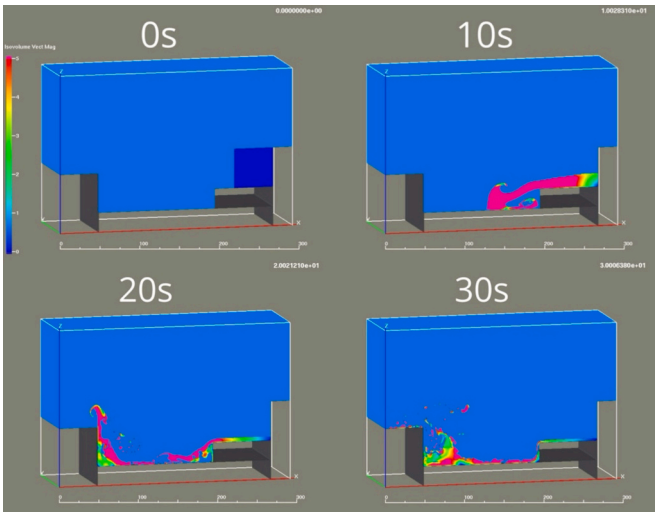

Fig. 5. Simulation results of the submarine landslide using SPLASH3D. The four panels represent sequential snapshots at 0, 10, 20, and 30 s. The colour within the landslide body represents the magnitude of velocity, which serves as an indicator of local kinetic energy and overall landslide dynamics.

Table 2
Landslide parameters.

	Duration time (*sec*)	Slope (°)	Length (m)	Width (m)	Thickness (m)
Toyama	20.0	70.0	500.0	80.0	40.0
Fushiki A	30.0	20.0	200.0	10.0	6.0
Fushiki B	30.0	30.0	250.0	25.0	9.0

6. Tsunami simulation results

6.1. Vertical displacement-generated tsunami

As shown in Fig. 6, when fault rupture occurs, the sea surface above the fault zone is uplifted, forming the initial tsunami source. Over time, the elevated water near the northeastern offshore area of the Noto Peninsula begins to propagate outward. At 7 min after the tsunami initiation (upper right panel of Fig. 6), a clear radial propagation pattern is observed. Toward the northeast, the wave height diminishes significantly. However, the waves traveling into Toyama Bay retain considerable amplitude.

This behavior is further illustrated in Fig. 7, which presents a cross-section of tsunami propagation a Toyama Bay. Near the bay mouth, the seafloor is relatively shallow—approximately 200 m deep—which amplifies the incident tsunami wave. At 7 min, the leading wave reaches this zone with a height of approximately 0.4 m and a wavelength of about 20 km. Upon entering Toyama Bay, the bathymetry deepens sharply to nearly 1200 m, causing the wave height to decrease to approximately 0.1 m while the wavelength doubles to around 40 km. This phenomenon is visible in both the bottom left panel of Fig. 6 and the corresponding cross-section in Fig. 7, taken 14 min after tsunami initiation.

By 21 min (bottom right of Fig. 7), the tsunami reaches the shallow coastal region. The rapid shoaling causes the wave height to increase again, ultimately producing wave heights of 0.3–0.4 m along the inner coast of Toyama Bay.

The two tsunami waveformplots (Fig. 8) show comparisons for the Toyama tide gauge station (upper) and the Fushiki tide gauge station (bottom). According to the simulation of the vertical displacement-generated tsunami, the first negative wave reached both stations approximately 10 min after the earthquake. Moreover, the simulated negative wave amplitude is relatively small.

However, the comparison with the observed data reveals a striking discrepancy: both Fushiki and Toyama stations recorded the arrival of the tsunami within 3 min of the earthquake. In both cases, the initial negative wave reached amplitudes of approximately 0.5 m, which is significantly larger than the simulated negative wave generated by

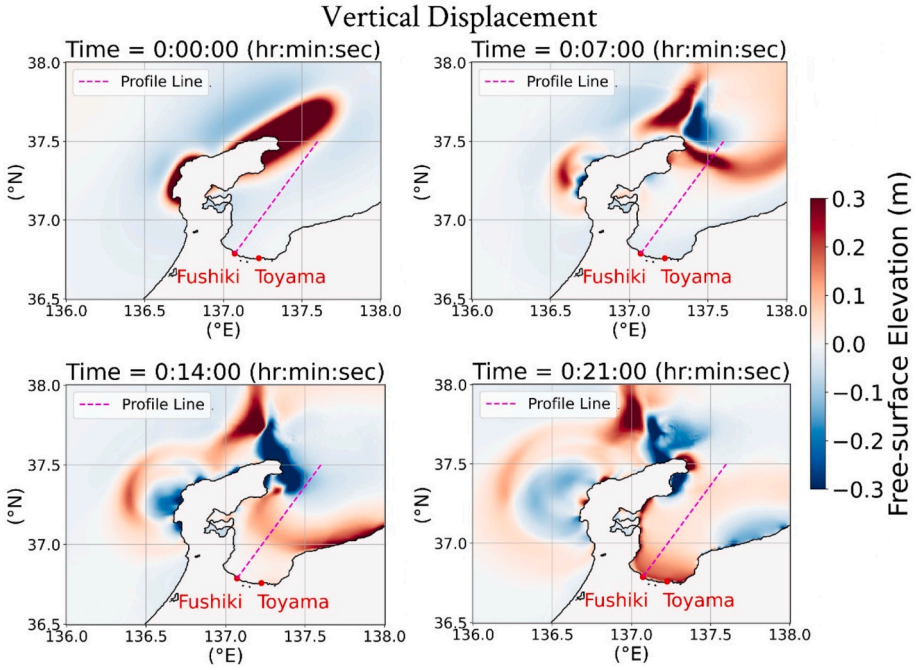

Fig. 6. Initial tsunami source and wave propagation of the vertical displacement-generated tsunami. The timestamps indicate elapsed time since the tsunami initiation, which is assumed to coincide with the earthquake occurrence.

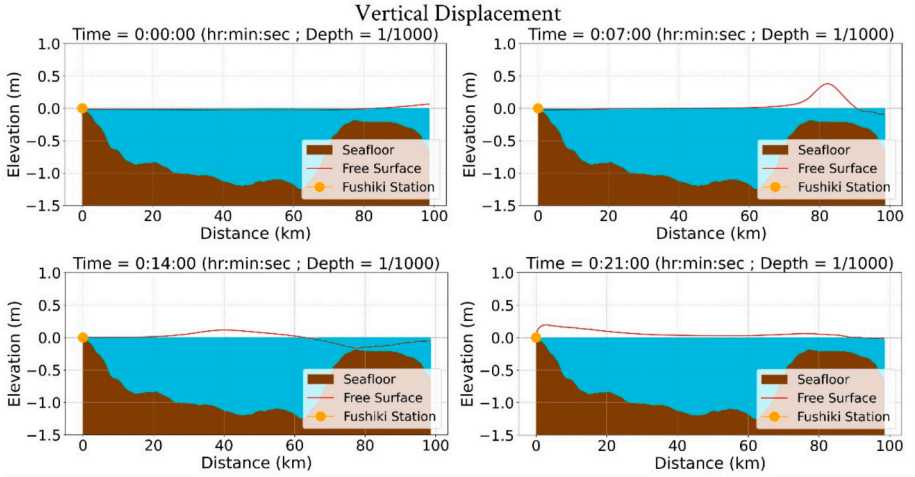

Fig. 7. Topographic cross-section and tsunami wave profile across Toyama Bay. The cross-section range corresponds to the line shown in Fig. 6. In this figure, the topographic elevation is vertically scaled by a factor of 1/1000, while tsunami wave amplitudes are shown at their original scale.

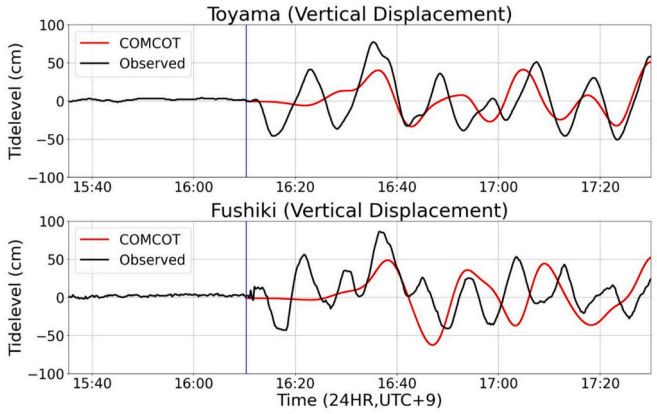

Fig. 8. Comparison between the observed tsunami waveforms at the Toyama and Fushiki tide gauge stations and the simulation results generated by vertical displacement. The blue vertical line indicates the earthquake origin time. (For interpretation of the references to colour in this figure legend, the reader is referred to the web version of this article.)

vertical fault displacement alone.

More importantly, the maximum wave height observed around 16:35 JST was approximately 0.8 m, clearly exceeding the simulated vertical displacement-generated tsunami peak of 0.4–0.5 m. Furthermore, the wave period derived from the earthquake tsunami simulation does not align well with the observed waveforms at either station.

These discrepancies strongly suggest that additional tsunami sources—beyond the vertical fault displacement—likely contributed to the observed tsunami signals. A combined effect of multiple sources may be responsible for the earlier arrival, higher wave amplitudes, and waveform differences observed at both tide gauge stations.

6.2. *Horizontal displacement-generated tsunami*

The initial source for the horizontal displacement-generated tsunami is an 80 cm horizontal displacement on the Noto Peninsula side (Fig. 9, upper left) at the steep bathymetry near the peninsula. As shown in the initial surface elevation plot (Fig. 9, upper left), the shape of the tsunami source reflects the underlying seafloor topography. The wave propagation pattern features overlapping concentric rings, which are caused by strong localized gradients in the initial surface displacement. These high- and low-energy zones act as secondary centers of wave radiation, producing multiple circular fronts.

Compared to the vertical displacement-generated tsunami, the wavelength of the horizontal displacement-generated tsunami is significantly shorter, which is clearly illustrated in the Toyama Bay cross-section (Fig. 10), where the horizontal displacement-generated tsunami displays a much shorter wavelength—approximately 5 km—than the vertical displacement-generated tsunami.

Simulation results show that the horizontal displacement-generated tsunami produced wave heights of about 10 cm at both the Toyama and Fushiki tide gauge stations. The two comparison plots in Fig. 11 show the simulated wave height versus the observed wave height. From these comparisons, it is evident that the simulated wave heights are much smaller than the observed values. Therefore, it is concluded that the tsunami generated by the 80 cm horizontal displacement on the Noto Peninsula side contributed little to the anomalous tsunami signals in this event and is unlikely to be a primary source of the early-arriving and high-amplitude waves.

As for the tsunami generated by the 10 cm horizontal displacement on the Toyama Prefecture side, the comparison between simulation results and observed data is shown in Fig. 12.

The simulated tsunami wave height is only about 1–2 cm, and the tsunami waveform in both comparison plots appears nearly flat, showing no significant variation, which indicates that the tsunami generated by the horizontal displacement of the Toyama Prefecture side had a negligible influence at either tide gauge station.

Therefore, the impact of the tsunami generated by the 10 cm horizontal displacement on the Toyama Prefecture side is considered insignificant, and it is excluded from further discussion in this study.

6.3. *Submarine landslide-generated tsunami*

The submarine landslide-generated tsunami simulation results are analyzed by examining the effect of each submarine landslide source on the nearest tide gauge station. Therefore, results for the Fushiki and Toyama stations are discussed separately.

Given that the epicentral distance from the Noto Peninsula to the landslide sites is approximately 80 km, and that seismic waves require some time to reach these locations, the landslide initiation time does not necessarily coincide with the earthquake origin time. In the tsunami waveform comparisons, the modeled results are aligned with observed data to determine the most reasonable onset time of the landslide within a physically plausible time window.

We determine the delay by aligning the first modeled crest (or trough) with the targeted crest (or trough) in the observations; the delay

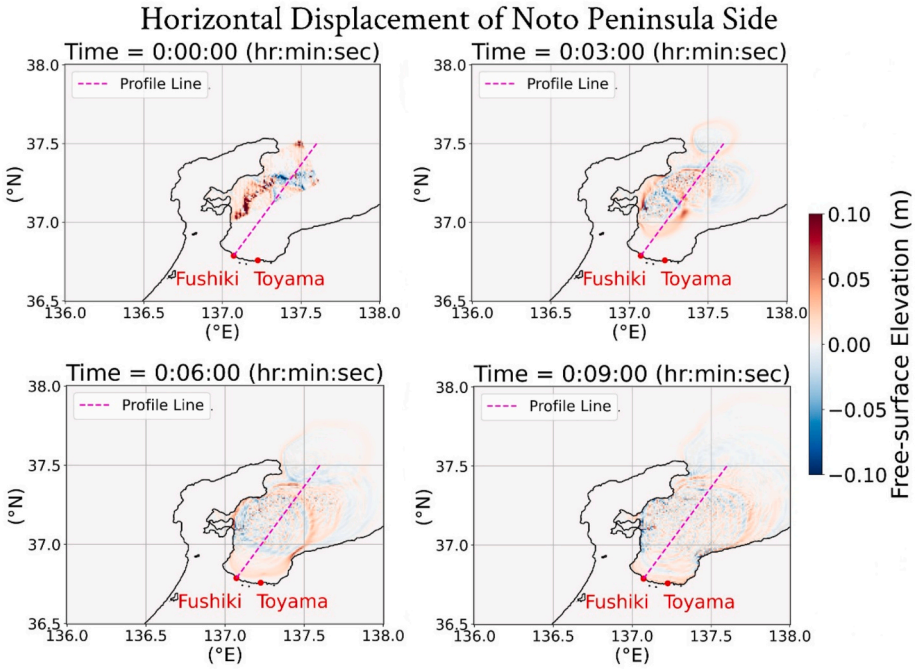

Fig. 9. The initial tsunami source and wave propagation were generated by the 80 cm horizontal displacement on the Noto Peninsula side. The timestamps indicate elapsed time since the tsunami initiation, which is assumed to coincide with the earthquake occurrence.

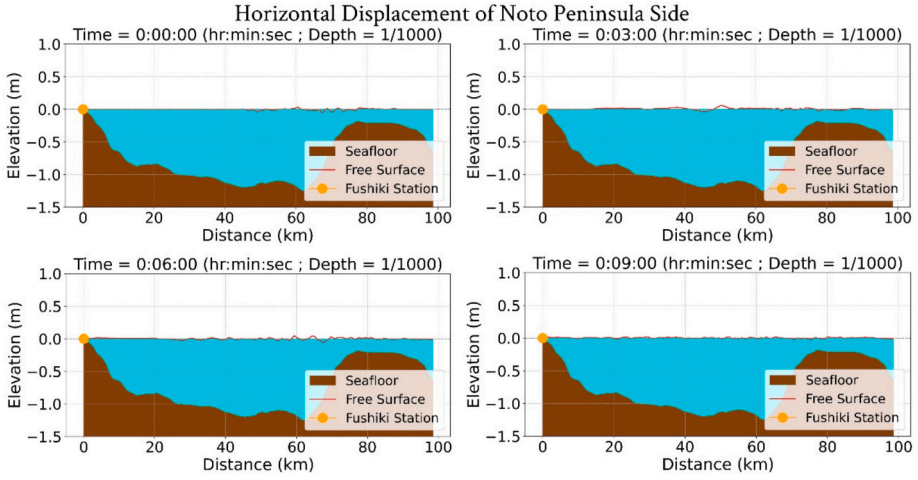

Fig. 10. Topographic cross-section and tsunami wave profile in Toyama Bay generated by the 80 cm horizontal displacement on the Noto Peninsula side. The cross-section range corresponds to the line shown in Fig. 9. In this figure, the topographic elevation is vertically scaled by a factor of 1/1000, while tsunami wave amplitudes are shown at their original scale.

obtained by this alignment, when combined with the vertical and horizontal displacement-generated tsunamis, most completely reproduces the tide-gauge records. The tsunami observations at the Toyama and Fushiki tide gauges have a sampling interval of 15 s. Based on the inferred landslide delay, a sensitivity test of linear wave superposition shows that when the added/subtracted time offset is within ±15 s, the agreement between the simulated waveforms and the observations changes only marginally.

6.3.1. Toyama tide gauge station (1 submarine landslide)

A submarine landslide scar was identified approximately 4 km north of the Toyama tide gauge station. Since the tsunami generated by the submarine landslide was modeled using a dynamic landslide source, Fig. 13 illustrates the free surface elevation and tsunami propagation from 1 to 4 min after the landslide onset. As shown in Fig. 13, the tsunami generated by the landslide reached the Toyama tide gauge station approximately 2 min after the start of the submarine landslide. Furthermore, the bottom-left panel of Fig. 13, which depicts the wavefield 4 min after the start of the submarine landslide, demonstrates that the wave amplitude decays rapidly after the termination of the landslide motion. As a result, the tsunami simulation for the landslide scenario in this study focuses on tide gauge stations that are nearest to the landslide source.

Fig. 14 presents a comparison between the simulated tsunami waveform based on this landslide scenario and the observed tide gauge data. In this simulation, the landslide initiation time was set to 105 s after the earthquake origin.

By examining the comparison in Fig. 14, it can be observed that when the landslide initiation time is set to 105 s after the earthquake, the resulting tsunami simulation successfully explains the early arrival of

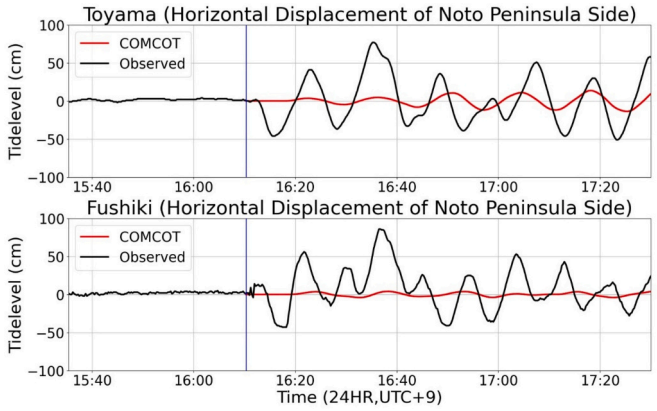

Fig. 11. Comparison between the observed tsunami waveforms at the Toyama and Fushiki tide gauge stations and the simulation results generated by the 80 cm horizontal displacement on the Noto Peninsula side. The blue vertical line indicates the earthquake origin time. (For interpretation of the references to colour in this figure legend, the reader is referred to the web version of this article.)

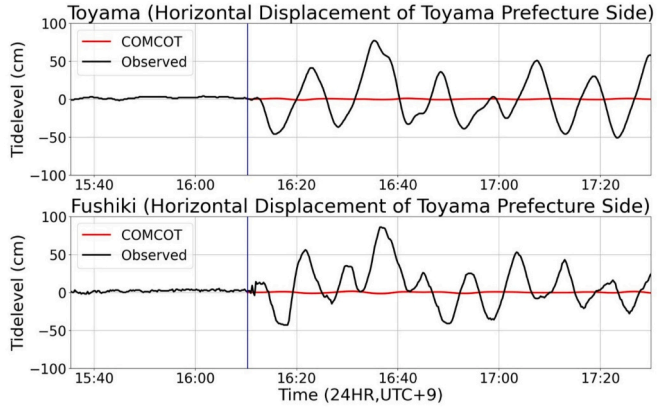

Fig. 12. Comparison between the observed tsunami waveforms at the Toyama and Fushiki tide gauge stations and the simulation results generated by the 10 cm horizontal displacement on the Toyama Prefecture side. The blue vertical line indicates the earthquake origin time. (For interpretation of the references to colour in this figure legend, the reader is referred to the web version of this article.)

the first wave trough at the Toyama tide gauge station. Additionally, the wave period produced by the landslide tsunami is closely aligned with the observed data.

These findings suggest that the landslide-generated tsunami significantly contributed to the anomalous tsunami observed at Toyama Station during the 2024 Noto earthquake event.

6.3.2. *Fushiki tide gauge station (2 submarine landslides)*

Similar to Toyama Station, submarine landslide scars were also identified within a 3 km radius of the Fushiki tide gauge station. Two distinct and prominent landslide features were observed near the station. We hypothesize that both landslides contributed to the anomalous tsunami signals recorded during this event.

Therefore, for the Fushiki station, we conducted a detailed analysis of the individual impact of each landslide source. By comparing the simulation results of both sources with the observed tide gauge data, we estimated the respective initiation times of the two landslides. We assessed their individual and combined contributions to the overall tsunami waveform.

Fig. 15 and Fig. 16 show the tsunami propagation patterns associated with Landslide A and Landslide B, respectively, both located near the Fushiki tide gauge station. The wave dynamics in both cases exhibit similar temporal and spatial patterns to those observed for the submarine landslide near the Toyama tide gauge station (Fig. 13). However, Landslide A and Landslide B are situated closer to the coastline and are smaller in scale compared to the landslide source near the Toyama tide gauge station.

The two figures above show a comparison between simulation results and observed tide gauge data for submarine landslide A (Fig. 17, upper) and landslide B (Fig. 17, middle) near Fushiki Station.

Simulation results reveal that the first wave generated by Landslide A was negative, while that generated by Landslide B was a positive wave. We interpret this contrast because of the differing sliding directions of the two submarine landslides, which influenced the waveform observed at the tide gauge station. Specifically, Landslide A slid southeastward, parallel to the coastline, whereas Landslide B moved southwestward, directly toward the shore (JCG, 2024b). Based on this, we infer that Landslide A occurred approximately 100 s after the earthquake, generating the first observed negative wave at the Fushiki tide gauge station (Fig. 17 upper). In contrast, Landslide B is estimated to have occurred 975 s after the earthquake, producing a positive initial wave that matches the positive waveform observed around 16:30. This latter signal cannot be explained by Landslide A alone (Fig. 17 middle).

Fig. 17 (bottom) shows the comparison between the combined tsunami waveform generated by submarine landslides A and B and the observed tide gauge data at Fushiki Station. In this simulation, Landslide A is assumed to occur 100 s after the earthquake, while Landslide B occurs 975 s after the earthquake.

By superimposing the waveforms from both events, the simulated tsunami closely matches the observed waveform in the early stages, supporting the interpretation that submarine landslides strongly influence the anomalous tsunami signals recorded at Fushiki Station.

6.4. *Combined effects of multiple tsunami sources*

By superimposing the tsunami waveforms generated by the three investigated sources vertical fault displacement, horizontal displacement on Noto Peninsula side, and submarine landslides (for each landslide source, its effect is considered only at the nearest tide gauge station) the resulting combined waveforms are shown in the comparison plots for Toyama Station (Fig. 18 upper) and Fushiki Station (Fig. 18 bottom).

The simulated waveforms exhibit a good agreement with the observed tide gauge data at both stations, particularly in terms of arrival time, wave amplitude, and waveform shape. These results strongly indicate that the tsunami signals recorded at Fushiki and Toyama during the 2024 Noto earthquake were not caused by a single source, but rather by the combined effects of multiple tsunami generation mechanisms.

7. Discussion

In this study, we conducted numerical simulations of tsunamis for multiple potential sources—including vertical fault displacement, horizontal displacement, and submarine landslides—to explain the anomalous tsunami behaviors observed at the Toyama and Fushiki tide gauge stations during the 2024 Noto Peninsula earthquake.

The successful simulation and analysis of nearshore landslide-generated tsunamis in this study can be primarily attributed to the use of SPLASH3D to determine the duration of landslide motion, followed by the implementation of the temporally variable seabed motion method in COMCOT. This approach enables the simulation of tsunamis generated by dynamically evolving landslide sources. Compared to the equivalent instantaneous initial free surface displacement method, it significantly improves the accuracy of tsunami modeling near the landslide source. Consequently, the contribution of each tsunami source to the 2024 event can be evaluated more comprehensively and intuitively.

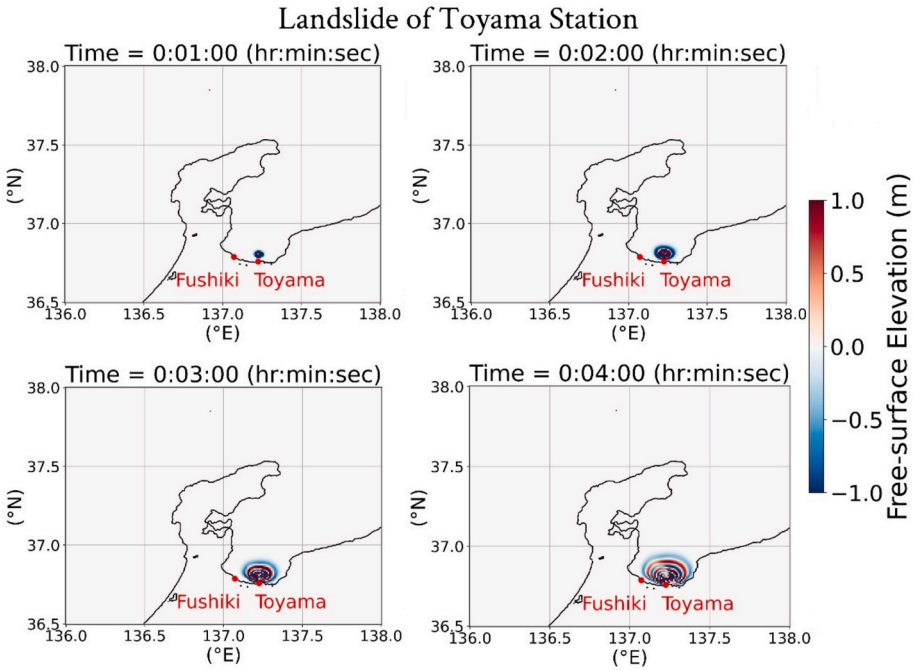

Fig. 13. Dynamic submarine landslide-generated tsunami source and wave propagation of submarine landslide near Toyama tide gauge station. The timestamps indicate elapsed time since the tsunami initiation, which is assumed to be 105 s after the earthquake occurrence.

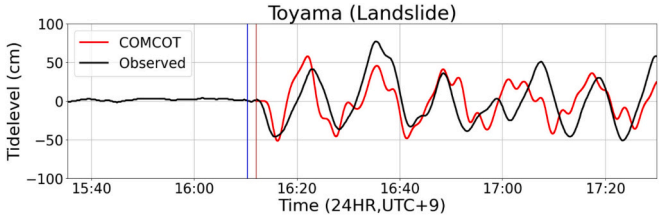

Fig. 14. Comparison between the observed tsunami waveforms at the Toyama tide-gauge station and the simulation results generated by a submarine landslide. The landslide is assumed to have occurred 4 km north of the station, with an initiation time of 105 s after the earthquake. The blue vertical line denotes the earthquake origin time; the brown line denotes the landslide initiation time. (For interpretation of the references to colour in this figure legend, the reader is referred to the web version of this article.)

The current integration strategy between the two models involves representing the landslide as a rectangular block and converting its motion into a free surface displacement using analytical formulas. This displacement is then used as the initial condition in a shallow water equation-based tsunami model. The future goal is to directly import the free surface condition from specific time steps of the three-dimensional fluid model into the tsunami model to enable hot-start simulations. Additionally, the plan includes incorporating realistic bathymetry and landslide geometry into the 3D fluid model, allowing for a more comprehensive representation of the landslide's dynamic behavior and making the tsunami source more physically realistic.

Furthermore, under nearshore conditions where nonlinear effects are more significant, long-duration simulations can lead to error accumulation, which is unfavorable when investigating tsunami behavior occurring long after the landslide event. In this study, a comparison between simulation results and observational data shows good agreement within the first 40 min after the landslide. However, beyond 40 min, noticeable deviations begin to appear, once again highlighting the impact of error accumulation on the latter parts of the simulation. Since this study focuses on the tsunami behavior within 40 min of the landslide occurrence, it is less affected by errors accumulation from nonlinear effects.

According to the simulation results, the early tsunami arrival times observed at both stations are primarily attributed to nearby submarine landslide sources, located just 3–5 km from the tide gauges. The simulations revealed that landslide-generated tsunamis could reach the closest tide stations within 2–3 min after the landslide onset.

We also considered the delayed initiation time of landslides relative to the earthquake origin. For the landslide located 4 km north of Toyama Station, a delay of 105 s provided the best fit to the observed waveform and accurately reproduced the early tsunami arrival. At Fushiki Station, two landslides were identified in the vicinity. Landslide A, simulated with an onset time of 100 s, effectively explained the first early-arriving wave; Landslide B, simulated at 975 s, matched the secondary wave amplification observed near 16:30 JST, and contributed to the overall waveform thereafter.

Regarding the larger-than-expected tsunami amplitudes observed at both stations between 16:30 and 17:00 JST, the combined-source simulations closely reproduced the maximum wave heights seen in the tide gauge data. In contrast, simulations with individual sources failed to reach such amplitudes. These results confirm that the combined effects of vertical displacement and landslide-generated tsunamis caused the enhanced wave heights. Based on waveform decomposition, the contributions of each were roughly equal—both for about 45 % of the observed waves—indicating that landslide tsunamis not only caused early arrival but also effectively doubled the observed tsunami heights.

Regarding the Noto Peninsula side horizontal displacement-generated tsunami, the simulations at both stations yielded wave heights of approximately 8 cm, accounting for about 10 % of the observed waves. Based on comparisons between simulation results and observational data, horizontal displacement is not considered the primary cause of the early tsunami arrivals and unexpectedly large wave amplitudes observed at both Toyama and Fushiki tide gauge stations during this event.

In this event, the observed tsunami waveform is primarily influenced by both vertical displacement and the submarine landslide. During the linear superposition of tsunami waveforms, we found that the delay time of the landslide significantly affects the resulting combined waveform.

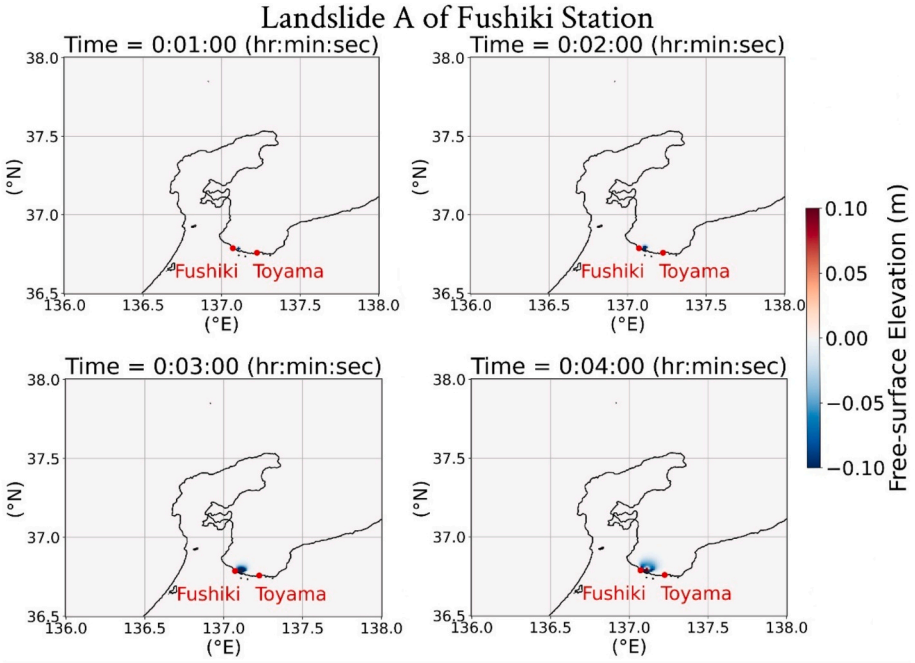

Fig. 15. Dynamic submarine landslide-generated tsunami source and wave propagation of submarine landslide A near the Fushiki tide gauge station. The timestamps indicate elapsed time since the tsunami initiation, which is assumed to be 100 s after the earthquake occurrence.

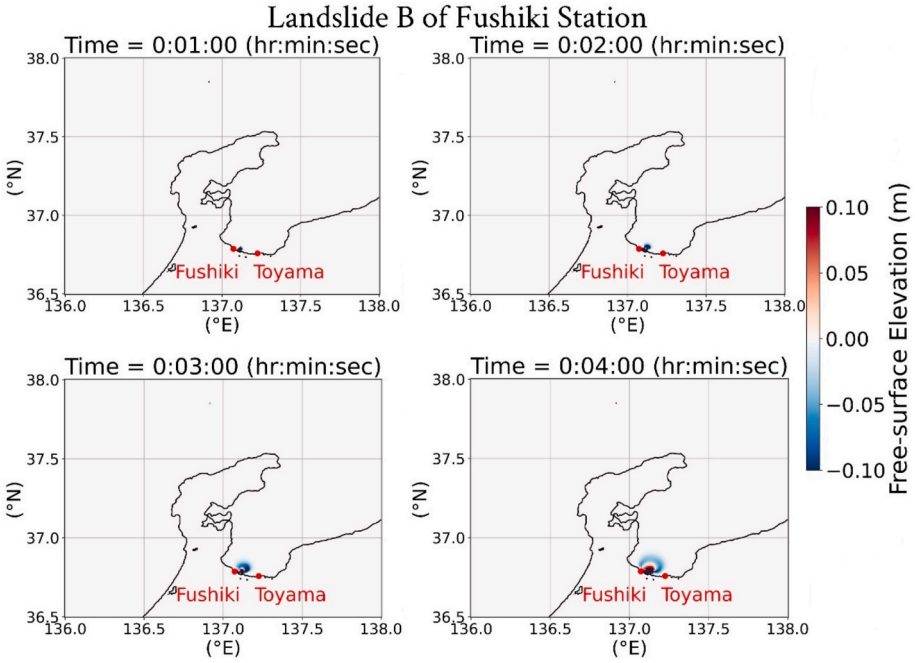

Fig. 16. Dynamic submarine landslide-generated tsunami source and wave propagation of submarine landslide B near the Fushiki tide gauge station. The timestamps indicate elapsed time since the tsunami initiation, which is assumed to be 975 s after the earthquake occurrence.

Under the selected delay time in this study, the wave crests of both the landslide-induced tsunami and the tsunami generated by vertical displacement arrive near the timing of the maximum observed wave height. The constructive interference between the two tsunami sources results in a higher-than-expected peak wave height at the Toyama and Fushiki tide gauge stations. However, at certain other delay times, the waveforms from the two sources can interfere destructively, leading to a maximum wave height that is lower than that produced by either source alone.

In summary, this study demonstrates that tsunami waves generated by submarine landslides during the 2024 Noto earthquake can significantly impact tsunami early warning systems, resulting in earlier-than-expected arrivals and underestimated wave heights. This poses substantial challenges for both tsunami early warning and coastal engineering risk assessment. We anticipate that our findings will help strengthen future practice: for early warning, agencies should conduct scenario simulations of submarine landslides of varying magnitudes in landslide-prone areas and evaluate the resulting arrival lead times and potential impacts; these results can then guide adjustments to evacuation strategies in regions susceptible to landslide-generated tsunamis to

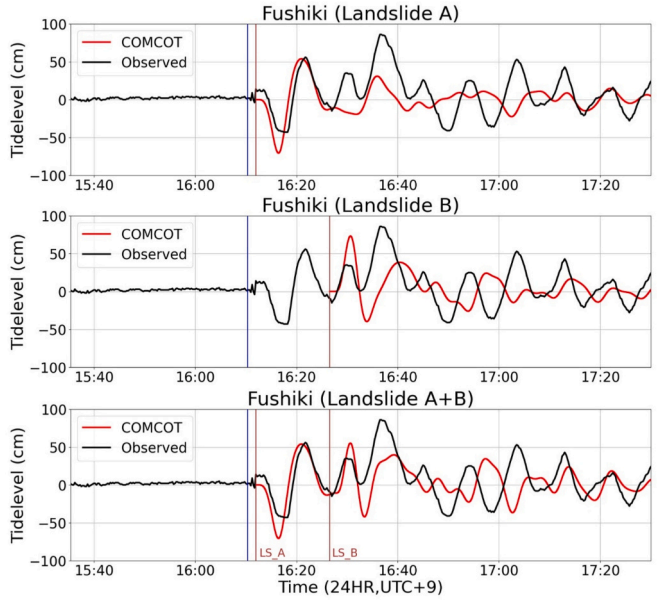

Fig. 17. Comparison between the observed tsunami waveforms at the Fushiki tide gauge station and the simulation results generated by submarine landslides A (upper), B (middle), and A + B (bottom). The simulation includes a delayed initiation of 100 s for landslide A and 975 s for landslide B. The blue vertical line denotes the earthquake origin time; the brown line denotes the landslide initiation time. (For interpretation of the references to colour in this figure legend, the reader is referred to the web version of this article.)

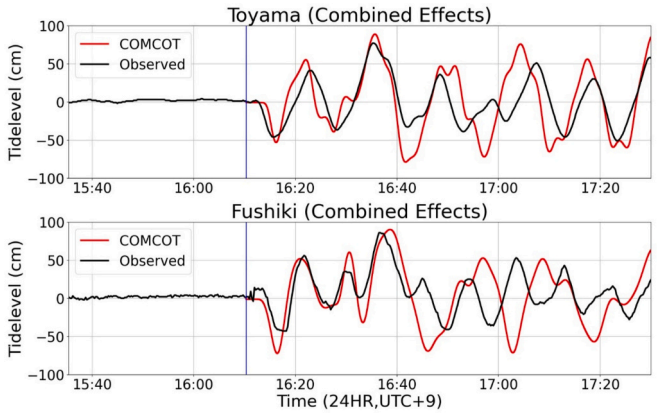

Fig. 18. Comparison between the observed tsunami waveforms at the Toyama and Fushiki tide gauge stations and the simulation results produced by the combined effects. The blue vertical line indicates the earthquake origin time. (For interpretation of the references to colour in this figure legend, the reader is referred to the web version of this article.)

minimize losses. Moreover, because the combined effects can produce maximum wave heights that exceed those predicted from vertical displacement from fault motion, coastal engineering risk assessments should explicitly account for the additional wave-height contributions from landslide-generated tsunamis.

8. Conclusions and implications for engineering geology

1. Early arrivals require local slides. The 2–3 min first detections at Toyama/Fushiki are best explained by proximal submarine landslides, not by fault displacement alone.
2. Combined sources control peak hazard. Constructive interference between submarine landslide-generated and fault-generated waves produced the largest peaks (16:30–17:00 JST). On average, each contributed about 45 % of observed amplitudes, while horizontal displacement accounted for only about 10 %.
3. Integration matters. A workflow that resolves slide duration in 3D model and drives a time-varying source in the propagation model improves near-field realism relative to instantaneous-displacement methods, enabling clearer source attribution and timing sensitivity tests.
4. Timing sensitivity is a hazard lever. Small changes in landslide onset can switch constructive or destructive interference at key sites, implying that scenario libraries for embayments should systematically sweep onset delays and slide positions.
5. Operational relevance. Because slide-augmented scenarios can arrive earlier and peak higher than fault-only forecasts, warning centers should pre-compute landslide scenario ensembles for known-prone areas and incorporate arrival lead-time envelopes and peak-height ranges into procedures and public messaging.

Practical recommendations

- Early warning: Maintain a library of slide-augmented scenarios (varying magnitude, location, onset delay) for Toyama Bay–type embayments; include site-specific arrival envelopes for critical tide stations and ports.
- Monitoring: Prioritize bathymetric change detection and slope-stability indicators at mapped submarine-landslide candidates to inform real-time scenario selection.
- Engineering design & risk: For near-field sites, adopt combined-source design waves rather than fault-only spectra; where feasible, translate peak depth/flux to damage metrics consistent with risk frameworks used in engineering practice.

CRediT authorship contribution statement

Ming-Jen Lo: Writing – review & editing, Writing – original draft, Visualization, Validation, Formal analysis, Data curation, Conceptualization. **Tso-Ren Wu:** Writing – review & editing, Supervision, Software, Resources, Project administration, Methodology, Funding acquisition, Conceptualization. **Kenji Satake:** Writing – review & editing, Supervision, Methodology, Conceptualization.

Declaration of competing interest

The authors declare the following financial interests/personal relationships which may be considered as potential competing interests:

Tso-Ren Wu reports financial support was provided by National Science and Technology Council. If there are other authors, they declare that they have no known competing financial interests or personal relationships that could have appeared to influence the work reported in this paper.

Acknowledgements

The authors would like to acknowledge the support from the Central Weather Administration, Ministry of Transportation and Communications, Taiwan, under project MOTC-CWA-114-E-03, “Scenario reconstructions of the 1920 and 0403 Hualien tsunami events and tsunami hazard assessment of Hualien area,” and from the National Science and Technology Council (NSTC), Taiwan, under project NSTC 113-2116-M-008-006, “Reconstruct the paleo-tsunamis induced by volcanic flank collapse and submarine landslides in the northern flank of the Kueishantao Island (III).” These projects are part of the Tsunami Science Research Group at the Hydrological and Oceanographic Sciences Research Institute, National Central University. Kenji Satake is supported by the Yushan Fellow Program from the Ministry of Education, Taiwan.

Data availability

The authors do not have permission to share data.

References

Abe, I., Goto, K., Imamura, F., et al., 2008. Numerical simulation of the tsunami generated by the 2007 Noto Hanto Earthquake and implications for unusual tidal surges observed in Toyama Bay. Earth Planets Space 60, 133–138. https://doi.org/10.1186/BF03352774.

Franco, A., Moernaut, J., Schneider-Muntau, B., Strasser, M., Gems, B., 2021. Triggers and consequences of landslide-induced impulse waves—3D dynamic reconstruction of the Taan Fiord 2015 tsunami event. Eng. Geol. 294, 106384. https://doi.org/10.1016/j.enggeo.2021.106384.

Fujii, Y., Satake, K., 2024. Slip distribution of the 2024 Noto Peninsula earthquake (MJMA 7.6) estimated from tsunami waveforms and GNSS data. Earth Planets Space 76, 44. https://doi.org/10.1186/s40623-024-01991-z.

GEBCO, 2023. https://www.gebco.net/.

Geospatial Information Authority of Japan (GSI), 2024. The 2024 Noto Peninsula Earthquake in Japanese Report of CCEP (Coordinating Committee of Earthquake Prediction), vol. 112, pp. 525–571. https://cais.gsi.go.jp/YOCHIREN/report/kaihou112/11_05.pdf.

Heidarzadeh, M., Ishibe, T., Gusman, A.R., Miyazaki, H., 2024. Field surveys of tsunami runup and damage following the January 2024 Mw 7.5 Noto (Japan Sea) tsunamigenic earthquake. Ocean Eng. 307, 118140. https://doi.org/10.1016/j.oceaneng.2024.118140.

Japan Coast Guard (JCG), 2024, January 24. Traces of Submarine Landslides Identified on Toyama Bay Seafloor (in Japanese). https://www.kaiho.mlit.go.jp/info/kouhou/r6/k240124/k240124.pdf.

Japan Coast Guard (JCG), 2024, December 2. Confirmation of Traces of Submarine Landslides on the Seafloor in Toyama Bay (3rd Report) - Submarine Landslides on the Seafloor off Fushiki, Takaoka City (in Japanese). https://www.kaiho.mlit.go.jp/info/kouhou/r6/k241202_1/k241202_1.pdf.

Japan Meteorological Agency (JMA), 2024. Earthquakes and Tsunami Reports at the Time of the Disaster: The 2024 Noto Peninsula Earthquake (in Japanese). https://www.jma.go.jp/jma/kishou/books/saigaiji/saigaiji_2024/saigaiji_202403.pdf.

Liu, P.L.-F., Cho, Y.-S., Briggs, M.J., Kanoglu, U., Synolakis, C.E., 1995. Runup of solitary waves on a circular Island. J. Fluid Mech. 302, 259–285. https://doi.org/10.1017/S0022112095004095.

Liu, J., Heller, V., Wang, Y., Yin, K., 2025. Investigation of subaerial landslide–tsunamis generated by different mass movement types using smoothed particle hydrodynamics. Eng. Geol. 352, 108055. https://doi.org/10.1016/j.enggeo.2025.108055.

Mulia, I.E., Heidarzadeh, M., Gusman, A.R., Satake, K., Fujii, Y., Sujatmiko, K.A., Meilano, I., Windupranata, W., 2024. Compounding impacts of the earthquake and submarine landslide on the Toyama Bay tsunami during the January 2024 Noto Peninsula event. Ocean Eng. 310 (Part 1), 118698. ISSN 0029-8018. https://doi.org/10.1016/j.oceaneng.2024.118698.

Okada, Y., 1985. Surface deformation due to shear and tensile faults in a half-space. Bull. Seismol. Soc. Am. 75 (4), 1135–1154. https://doi.org/10.1785/BSSA0750041135.

Tanioka, Y., Satake, K., 1996. Tsunami generation by horizontal displacement of ocean bottom. Geophys. Res. Lett. 23 (8), 861–864. https://doi.org/10.1029/96GL00736.

The Association of Japanese Geographers, 2024. Results of Investigation of Tsunami Inundation Extent by the 2024 Noto Peninsula Earthquake (fourth Report) (in Japanese). https://disaster.ajg.or.jp/files/202401_Noto009.pdf.

University of Toyama, 2025. Direct Observation of a “Submarine Landslide” Site in the Southern Part of Toyama Bay Using an Underwater Drone (in Japanese). https://www.u-toyama.ac.jp/wp/wp-content/uploads/20250116.pdf.

Wang, X., Liu, P.L., 2005. A numerical investigation of Boumerdes-Zemmouri (Algeria) earthquake and tsunami. Comput. Model. Eng. Sci. 10 (2), 171–184. https://doi.org/10.3970/cmes.2005.010.171.

Wang, J., Ward, S.N., Xiao, L., 2019. Tsunami Squares modeling of landslide generated impulsive waves and its application to the 1792 Unzen–Mayuyama mega-slide in Japan. Eng. Geol. 256, 121–137. https://doi.org/10.1016/j.enggeo.2019.04.020.

Wang, J., Xiao, L., Ward, S.N., Du, J., 2021. Tsunami Squares modeling of the 2007 Dayantang landslide-generated waves considering the effects in slide/water interactions. Eng. Geol. 284, 106032. https://doi.org/10.1016/j.enggeo.2021.106032.

Watts, P., Grilli, S.T., Kirby, J.T., Fryer, G.J., Tappin, D.R., 2003. Landslide tsunami case studies using a Boussinesq model and a fully nonlinear tsunami generation model. Nat. Hazards Earth Syst. Sci. 3, 391–402. https://doi.org/10.5194/nhess-3-391-2003.

Wu, T.-R., 2004. A Numerical Study of Three-Dimensional Breaking Waves and Turbulence Effects. Cornell University. https://tsunami.ihs.ncu.edu.tw/study/paper/Tso-Ren%27sdissertation.pdf.

Wu, T.R., Chen, P.F., Tsai, W.T., Chen, G.Y., 2008. Numerical study on tsunamis excited by 2006 Pingtung earthquake doublet. Terr. Atmos. Ocean. Sci. 19, 705–715. https://doi.org/10.3319/TAO.2008.19.6.705(PT).

Yanagisawa, H., Abe, I., Baba, T., 2024. What was the source of the nonseismic tsunami that occurred in Toyama Bay during the 2024 Noto Peninsula earthquake? Sci. Rep. https://doi.org/10.21203/rs.3.rs-4407969/v1.

Yuhi, M., Umeda, S., Arita, M., Ninomiya, J., Gokon, H., Arikawa, T., Mori, N., 2024. Post-event survey of the 2024 Noto Peninsula earthquake tsunami in Japan. Coast. Eng. J. 66 (3), 405–418. https://doi.org/10.1080/21664250.2024.2368955.